https://doi.org/10.5194/wes-2025-10
Preprint. Discussion started: 31 January 2025

eawe european academy of wind energy
Open Access WIND ENERGY SCIENCE DISCUSSIONS

Non-linear interaction between synchronous generator and GFM controlled wind turbines - Inertial effect enhancement and oscillations mitigation

Chinmayi Wagh[1], Johan Boukhenfouf[1], Frédéric Colas[1], Luis Rouco[2], and Xavier Guillaud[1]

[1]Univ. Lille, Arts et Metiers Institute of Technology, Centrale Lille, Junia, ULR 2697 - L2EP, F-59000 Lille, France
[2]ETS ICAI-IIT, Universidad Pontificia Comillas, 28015 Madrid, Spain

Correspondence: Chinmayi Wagh (chinmayi.wagh@centralelille.fr)

Abstract. The integration of grid-forming (GFM) controlled wind turbines into AC grids introduces complex dynamic interactions that significantly influence its behavior on the AC side. This study explores the nonlinear coupling between wind turbines and AC grids and propose strategies for the enhancement of the inertial effect and the mitigation of oscillations which can arise in case of an AC event. A simplified synthetic model is developed to elucidate the physical insights of these interactions. The findings reveal that wind turbine dynamics has an impact on the inertial contribution and introduce oscillatory behavior under certain conditions. Advanced control strategies are then proposed. They include the integration of input shaping filters and lead-lag compensation to optimize inertial response and dampen mechanical oscillations. The theoretical analysis, validated through simulation, demonstrates the effectiveness and limitations of these methods in enhancing the AC side behavior without compromising the performance of the mechanical system.

1 Introduction

In the twentieth century, the electrical power system has a significant global development and most of the operational principles ensuring the system's stability were established based on the behavior of synchronous machines. The phenomenon of the inertial effect plays a crucial role in stabilizing the grid. A key consequence is the limitation of the Rate of Change of Frequency when a significant unbalance between the equilibrium between production and consumption occurs. Moreover, since all the rotating speeds of the machine are linked with the grid frequency, the imbalance between production and consumption is naturally propagated all over the grid through the frequency. Then, the frequency droop control allows the primary power of multiple power plants, distributed across a wide geographic area, to be adjusted in order to recover the balance. In summary, the synchronization process of these devices is creating couplings between the grid dynamics and the power sources dynamics which are beneficial to the grid frequency stability.

The emergence of inverter-based resources (IBRs) has brought significant changes in the power system analysis. Indeed, the grid following control which was the fundamental principle used to drive the control of these converters is based on a completely different principle. The Phase Locked Loop (PLL) allows to estimate the grid angle in real time such as it is possible to exchange an active and reactive power nearly independently from the grid frequency. The PLL breaks the beneficial coupling

https://doi.org/10.5194/wes-2025-10
Preprint. Discussion started: 31 January 2025

eawe european academy of wind energy
Open Access WIND ENERGY SCIENCE DISCUSSIONS

for the grid that exists in the synchronous machine. In case of a wind turbine, it is possible to recreate a kind of "artificial" inertial effect. Indeed, the inertial response comes from changing the active power with respect to frequency deviation that utilizes the kinetic energy stored in mechanical part of wind turbine. Various inertial control methods for wind power generation have been discussed for several years [(Morren et al., 2006), (Wu et al., 2018)]. In addition to standard natural, step-wise and virtual inertial controls for wind turbine optimized design of MPPT control (Wu et al., 2016) or optimized operation of phase lock loop (Hu et al., 2016) provides improved inertial response with temporarily enhanced frequency support. However, this operation needs to derivate the grid frequency, which can introduce delays due to the necessary filtering applied to mitigate measurement noise.

(Cardozo et al., 2024) highlights the limits of grid following solutions to fulfill the fundamental systems needs to guarantee a stable behaviour for the grid. It is the reason why the TSOs proposed to switch from grid following to grid forming control for the control of the IBRs. Indeed, some of the beneficial properties of the synchronous machine can be recovered and even sometime surpassed with such control. In Europe, ENTSOE has published a report which specifies the different requirements for the grid forming control (ENTSOE, 2017). In UK, a best practice guide has been proposed (ESO, 2023) and in the US, EPRI has also published a paper which defines the performance required for the grid forming control (Ramasubramanian et al., 2023). This non exhaustive list highlights the critical role of grid-forming control in various power grids worldwide.

Different types of grid forming control methodologies were proposed. Droop control, synchronous machine-based control and other controls are summarized in [(Rathnayake et al., 2021), (Rosso et al., 2021)]. In the case of a virtual synchronous machine (VSM) control, the virtual inertia and damping coefficient are design parameters unlike the inherent parameters of synchronous machine. Thanks to a stronger damping coefficient, the Grid Forming control (GFM) can damp inter-area oscillation [(Baruwa and Fazeli, 2021), (Xue et al., 2024)]. However, in all these studies, the DC bus voltage is considered as constant. When a wind turbine is connected to the DC bus, new types of dynamic couplings can be created. On the AC side, the electromechanical coupling between the grid and the mechanical part of the wind turbine modifies the inertial effect brought to the grid in case of a frequency variation (Xi et al., 2018). On the wind turbine side, the disturbance induced by the inertial effect is propagated to the mechanical structure of wind turbine through variations in the electromechanical torque. Two solutions can be proposed to mitigate this effect either by adding a damping effect on the electromechanical torque [(Avazov, 2022), (Chen et al., 2022)] but this may lead to a weaker DC bus voltage control or, by increasing the damping coefficient on the grid forming (Tessaro and de Oliveira, 2019) but this decreases the effectiveness of inertial response. In (Heidary Yazdi et al., 2019), a model highlighting the coupling between the grid and the wind turbine has been proposed for operation in MPPT region and one-mass wind turbine. Insights on electromechanical couplings are thus restricted.

This paper aims to provide a theoretical analysis of the new type of coupling dynamics arising from the interaction between wind turbine grid-forming controls and the power grid. A simplified synthetic model is proposed in section 3 which highlights the main couplings and allow for the development of some physical insights on this system. In section 4 it is shown that it is possible to act on the control to mitigate the unwanted dynamic behavior.

https://doi.org/10.5194/wes-2025-10
Preprint. Discussion started: 31 January 2025

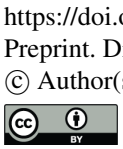

eawe european academy of wind energy
Open Access WIND ENERGY SCIENCE DISCUSSIONS

2 Non-linear model of the system

This section introduces the non-linear model of the test case used for EMT simulation to study system dynamics. It consists of 900MVA synchronous generator and a 900MVA aggregated wind farm (Shafiu et al., 2006) under grid forming control both supplying a load. The wind farm consists of 180 type IV wind turbines of 5MW. Figure 1 shows the model including the control loops of both machines. The detailed models of each component are presented in the following sections.

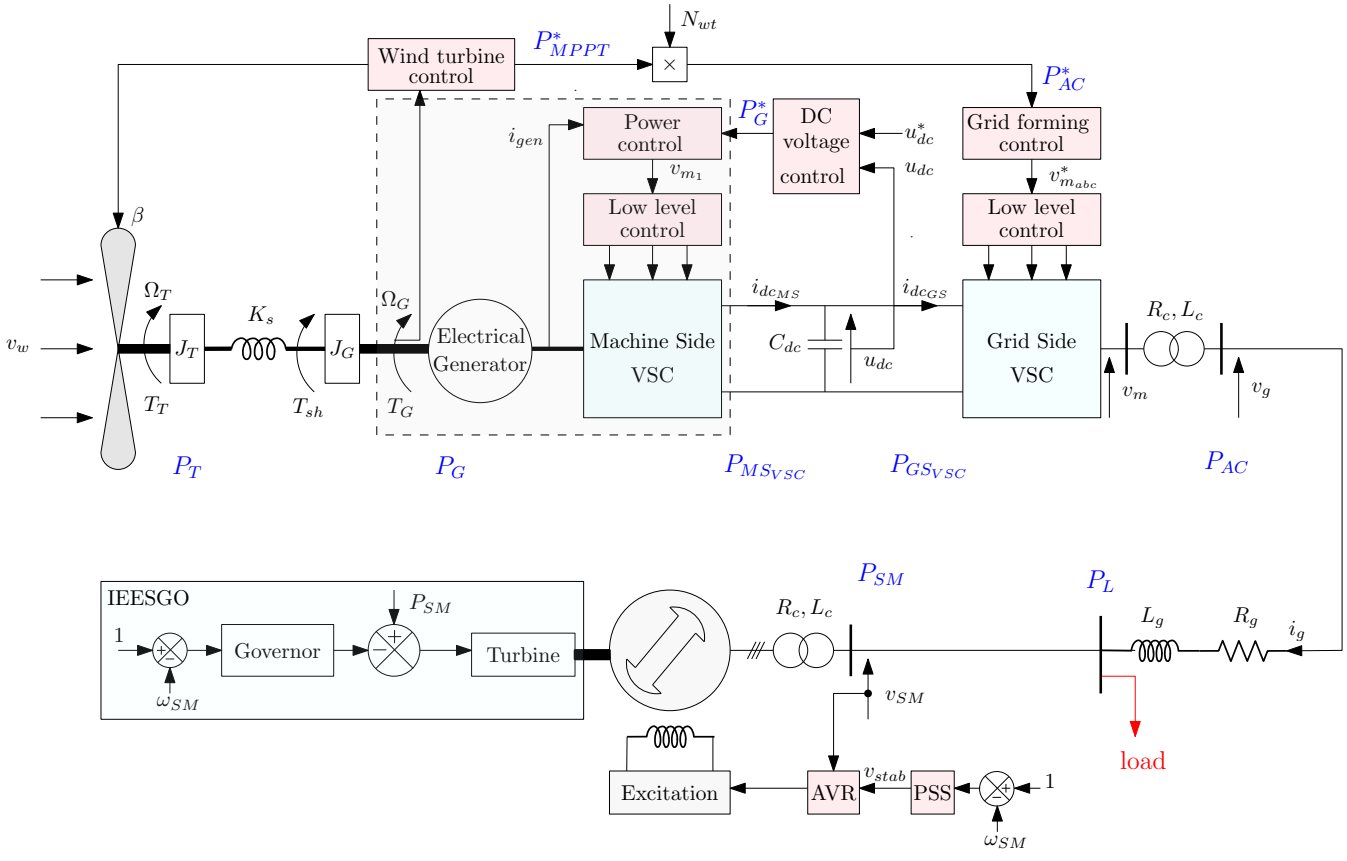

Figure 1. Overall system under study

2.1 Model of the wind turbine

The wind turbine model comprises several elements that describe either the power part or the control. The detailed presentation of these elements can be found in the next subsections.

https://doi.org/10.5194/wes-2025-10
Preprint. Discussion started: 31 January 2025

eawe european academy of wind energy
Open Access WIND ENERGY SCIENCE DISCUSSIONS

2.1.1 Mechanical model

The aerodynamic power is converted to mechanical power P_T given by Eq. (1) where R represents the wind turbine blades having radius and ρ the air density.

$$P_T = \frac{1}{2}\rho\pi R^2 c_p\left(\lambda,\beta\right) v_w^3 \tag{1}$$

The power coefficient $c_p(\lambda,\beta)$ is derived from the tip speed ratio λ and pitch angle β using Eq.(2).

$$c_p = 0.73\left(\frac{151}{\lambda_r} - 0.58\beta - 0.002\beta^{2.14} - 13.2\right)e^{\frac{-18.4}{\lambda_r}} \tag{2}$$

where, $\lambda_r = \frac{1}{\lambda - 0.1\beta} - \frac{0.003}{\beta^3+1}$ and $\lambda = \frac{R\Omega_T}{v_w}$ with Ω_T as the wind turbine rotational speed and v_w the wind speed. To illustrate, Fig.3a depicts the variation of power coefficient as a function of λ with $\beta = 0$.

Therefore, from P_T it is possible to derive the mechanical torque on wind turbine T_T:

$$T_T = \frac{P_T}{\Omega_T} \tag{3}$$

Considering Ω_G as the rotational speed of the generator and T_G as the torque of the generator, Ω_T and Ω_G are derived from the two-mass mechanical model Eq.(4-6) where J_T is the turbine inertia constant, J_G the generator inertia constant, T_{sh} the torque on the shaft, K_s for shaft stiffness and D_s damping coefficient.

$$\frac{d\Omega_T}{dt} = \frac{1}{J_T}(T_T - T_{sh}) \tag{4}$$

$$\frac{d\Omega_G}{dt} = \frac{1}{J_G}(T_{sh} - T_G) \tag{5}$$

$$\frac{dT_{sh}}{dt} = D_s\frac{d\Delta\omega}{dt} + K_s\Delta\omega \tag{6}$$

Considering the nominal power P_{nom} as the base power P_b, and the nominal speed Ω_{nom} as the base speed Ω_b, the per unit value of the inertia is introduced as $H_T = \frac{0.5J_T\Omega_b^2}{P_b}$ and $H_G = \frac{0.5J_G\Omega_b^2}{P_b}$ for the wind turbine and the generator respectively. A per unit coefficient is also introduced for the shaft stifness $K_s^{pu} = \frac{K_s\Omega_b^2}{P_b}$ and the damping coefficient $D_s^{pu} = \frac{D_s\Omega_b^2}{P_b}$. Therefore, Eq.(5) and Eq.(6) can be converted into their per-unit forms:

$$\frac{dT_{sh_{pu}}}{dt} = D_s^{pu}\frac{d\Delta\omega_{pu}}{dt} + K_s^{pu}\Delta\omega_{pu} \tag{7}$$

$$\frac{d\Omega_{T_{pu}}}{dt} = \frac{1}{2H_T}(T_{T_{pu}} - T_{sh_{pu}}) \tag{8}$$

$$\frac{d\Omega_{G_{pu}}}{dt} = \frac{1}{2H_G}(T_{sh_{pu}} - T_{G_{pu}}) \tag{9}$$

For simplicity, the subscript 'pu' for per unit is disregarded throughout the paper. Hence, Fig.2 represents the per-unit mechanical model of wind turbine based on Eq.(7)-Eq. (9).

https://doi.org/10.5194/wes-2025-10
Preprint. Discussion started: 31 January 2025

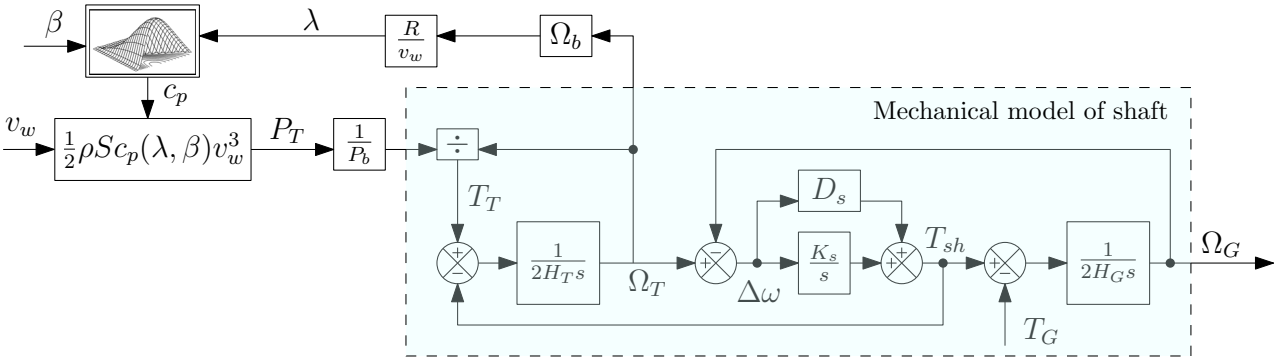

Figure 2. 2-mass per unit mechanical model of wind turbine

Additionally, a simplified model can be introduced by neglecting the oscillatory behavior of the turbine. This approach uses a per-unit one-mass mechanical model, where $\Omega_{1\text{mass}}$ represents the common rotational speed of both the wind turbine and the generator. Considering their equivalent inertia $H_{1mass} = H_T + H_G$, the shaft is then modeled as:

$$\frac{d\Omega_{1mass}}{dt} = \frac{1}{2H_{1mass}}(T_T - T_G) \tag{10}$$

2.1.2 Wind power conversion strategy and optimization

The power curve of wind turbine has various operating regions (Wu et al., 2016)-(Krpan and Kuzle, 2018) represented in Fig.3b in per-unit.

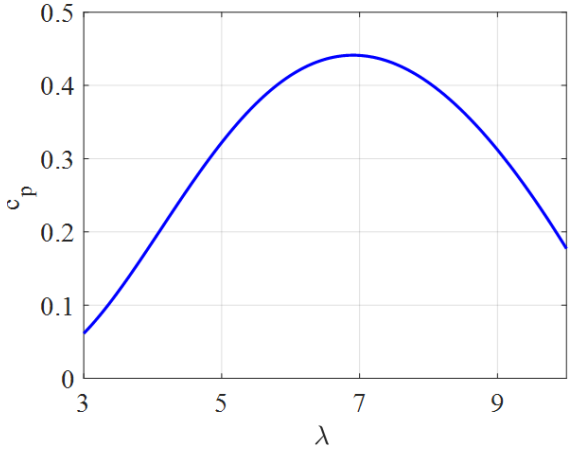

(a) cp curve

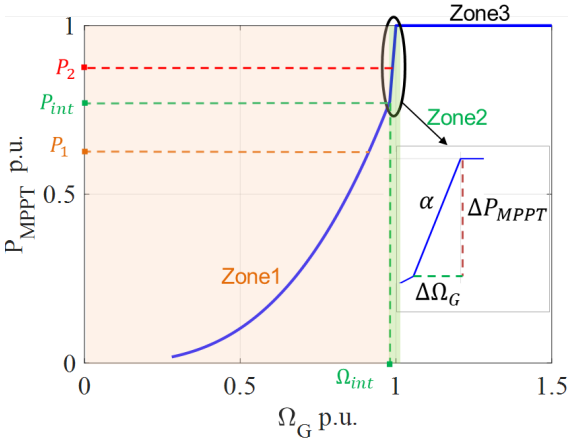

(b) Maximum power point tracking (MPPT) control

Figure 3. Wind turbine characteristic curves

https://doi.org/10.5194/wes-2025-10
Preprint. Discussion started: 31 January 2025

eawe european academy of wind energy
Open Access WIND ENERGY SCIENCE DISCUSSIONS

In the Maximum Power Point Tracking (MPPT) region referred as Zone 1, it is possible to define an optimal speed for each wind speed v_w to optimize the power generation. This optimal speed is reached by adjusting the generator torque T_G. In this operation mode, the power coefficient and tip-speed ratio have a constant value: c_{opt}, λ_{opt} . The maximum power P_{zone1} is given by Eq.(11).

$$P_{zone1} = \frac{1}{2P_b}\rho\pi R^2 c_{p_{opt}} \left(\frac{\Omega_G \Omega_b R}{\lambda_{opt}}\right)^3 \tag{11}$$

After a given wind speed, the MPPT cannot be applied anymore because the nominal rotation speed is reached. Then, the reference power applied aims to stay around the nominal speed, this operation mode is referred as speed limitation: zone 2 between two points (P_{int}, Ω_{int}) and (1,1) with slope $\alpha = \frac{1-P_{int}}{1-\Omega_{int}}$.Then the power P_{zone2} with the slope α is derived as:

$$P_{zone2} = \alpha(\Omega_G - \Omega_{int}) + P_{int} \tag{12}$$

Finally, when the nominal power is reached, the speed cannot be limited by the reference power anymore, the pitch control is actuated to decrease c_p and limit the power generated by the blades to its nominal value. Hence, named as power limitation: zone 3 with power P_{zone3} :

$$P_{zone3} = 1 \tag{13}$$

In summary, the operating point of the wind turbine determines the power output P^*_{MPPT} of the MPPT control given by Eq.(11) or Eq.(12) or Eq.(13) represented in Fig.4.

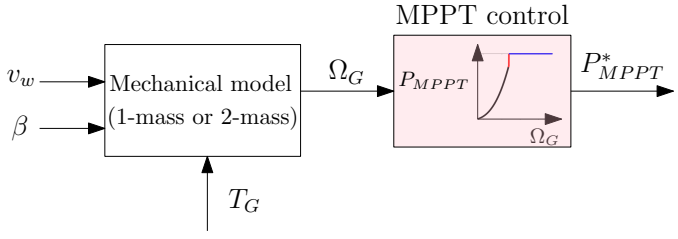

Figure 4. Wind turbine MPPT control

2.1.3 Model of the machine, machine side VSC and their controls

The generator and machine side VSC are considered lossless; therefore the generator power P_G and power delivered by machine side VSC $P_{MS_{VSC}}$ to DC bus are expressed by Eq.(14) with DC bus voltage u_{dc} and DC current $i_{dc_{MS}}$ injected into the DC bus.

$$T_G\Omega_G = P_G = P_{MS_{VSC}} = u_{dc} i_{dc_{MS}} \tag{14}$$

The electrical power is controlled to a reference value P^*_G thanks to a current loop. Due to the fast dynamics of the control, it can be written that:

$$P_G = P^*_G \tag{15}$$

https://doi.org/10.5194/wes-2025-10
Preprint. Discussion started: 31 January 2025

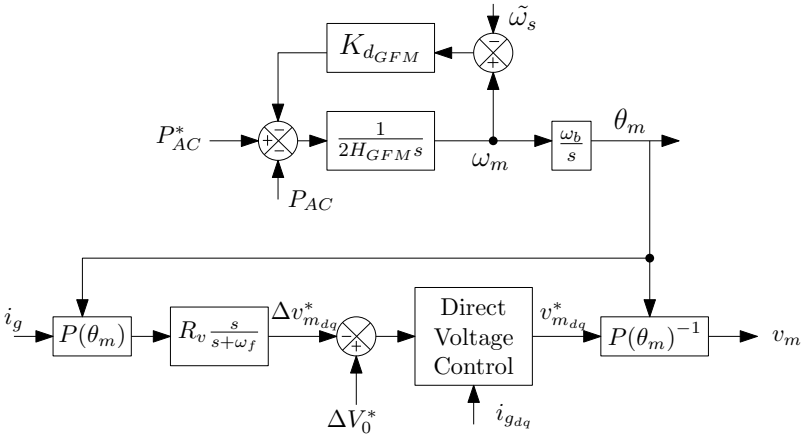

Figure 5. Reference model of grid-forming converter

Hence the DC current $i_{dc_{MS}}$ generated by the machine side VSC is calculated by Eq.(16).

$$i_{dc_{MS}} = \frac{P^*_G}{u_{dc}} \tag{16}$$

And equivalent power $P_{G_{eq}}$ generated by N_{wt} number of wind turbine is:

$$P_{G_{eq}} = P_G N_{wt} \tag{17}$$

2.1.4 Grid side VSC model and control

The system is connected to the grid thanks to a VSC. An average model of VSC is considered and the control is a Grid Forming. The converter modulates the DC bus voltage in order to generate the three-phase voltage v_{ma}, v_{mb}, v_{mc}. The Grid Forming Virtual synchronous machine (VSM) scheme Fig.5 is controlling the active power P_{AC} to match the reference P^*_{AC} by acting on the modulated voltage reference angle θ_m. The magnitude of the modulated voltage is set to V^*. In order to damp the current oscillations (Lamrani et al., 2023) a Transient Virtual Resistor (TVR) R_v modifies the voltage reference $v^*_{m_{dq0}}$. Then the reference modulated $v^*_{ma}, v^*_{mb}, v^*_{mc}$ are calculated by inverse of Park transformation $P(\theta_m)^{-1}$. Similar to the machine side converter, the grid side converter is assumed lossless with $P_{GS_{MSC}}$ the power exchanged between DC bus and grid side VSC given by:

$$P_{GS_{MSC}} = P_{AC} \tag{18}$$

2.1.5 DC bus model and control

The DC bus is modeled using a simple capacitor C_{dc} as:

$$C_{dc}\frac{du_{dc}}{dt} = i_{dc_{MS}} - i_{dc_{GS}} \tag{19}$$

https://doi.org/10.5194/wes-2025-10
Preprint. Discussion started: 31 January 2025

eawe european academy of wind energy
Open Access WIND ENERGY SCIENCE DISCUSSIONS

As for the inertia, it is possible to define an H value: $H_{dc} = \frac{C_{dc} V_{dc_b}^2}{2P_b}$ where V_{dc_b} is the base DC voltage equal to the nominal voltage of the DC bus. Hence, the DC bus model in per unit with inertia H_{dc} is expressed as:

$$\frac{du_{dc}^2}{dt} = \frac{1}{H_{dc}}(P_G - P_{AC}) \tag{20}$$

The DC bus control is needed to achieve the stability of the DC bus which depends on the power delivered by the generator side VSC (P_G) and the grid side VSC (P_{AC}). As shown in (Avazov, 2022) - (Huang et al., 2023), it is better to control the DC bus voltage by a direct action on the generator power. The DC bus voltage control is based on PI controller.

Hence the output of the DC bus controller is the reference for the generator P_G^* and the reference power of the GFM controller P_{AC}^* for N_{wt} number of wind turbines is derived from Eq.(15) and Eq.(17) as following :

$$P_{AC}^* = P_{G_{eq}} = P_{MPPT}^* N_{wt} \tag{21}$$

2.2 Synchronous machine model

A round rotor type 900MW synchronous machine is modeled using a detailed eighth-order model (P.Kundur, 1994) with H_{SM} as the inertia of synchronous machine and $K_{d_{SM}}$ as the damping coefficient. As illustrated in Fig.1 it is equipped with the following:

- a transformer with a resistance R_c and a leakage impedance L_c
- an excitation system of type ST1C (exc, 2016) that consist of main voltage regulator with gain K_a, a low-pass filter with time constant τ_r and input voltage v_{stab} from power system stabilizer
- a governor modeled as IEESGO (Pourbeik et al., 2013) with power frequency droop gain K_{pf} and low-pass filters with τ_1 and τ_3 representing the governor dynamics. A three-stage steam turbine is considered with output power P_{hp}, P_{ip}, P_{lp} and a low pass filter with τ_4 to include the dynamics of steam valve demonstrated in Fig.6.
- a powers system stabilizer model PSS1A(exc, 2016) that consist of two lead-lag filters, one wash-out filter $\tau_{p5} = 10s$, one low pass filter $\tau_{p6} = 0.01s$ and PSS gain $K_{PSS} = 0$

3 Linear models of the system

In order to use the classical tool for dynamic analysis, such as eigenvalues, a linear model is needed. This involves developing a linearized representation of the wind turbine and its control system. Merging this linearized model with the linearized model of the synchronous machine leads to a linearized model of the system described in Fig.1. By introducing a few additional assumptions, a simplified linearized model can be derived. This simplified model, represented as a block diagram, provides valuable physical insight into the dynamics of the system

https://doi.org/10.5194/wes-2025-10
Preprint. Discussion started: 31 January 2025

eawe european academy of wind energy
Open Access WIND ENERGY SCIENCE DISCUSSIONS

3.1 Reference Linear model

The first linear model consists of:

1. Linearized model of wind turbine: It is obtained by linearizing P_T Eq.(1) in two components $\frac{dP_T}{dv_w}$ positive value for all operating points and $\frac{dP_T}{d\Omega_G}$ negative value for all operating points. Even with this simplification, some non-linearities remain in the model. The gain K_{MPPT} represents the power characteristics to generate ΔP^*_{MPPT}:
   (a) In zone1 by linearizing Eq.(11),$\Delta P^*_{MPPT} = \Delta P_{zone1}$ and $K_{MPPT} = \frac{dP_{zone1}}{d\Omega_G}$
   (b) In zone2 by linearizing Eq.(12),$\Delta P^*_{MPPT} = \Delta P_{zone2}$ and $K_{MPPT} = \alpha$
   (c) In zone3 by linearizing Eq.(13),$\Delta P^*_{MPPT} = \Delta P_{zone3}$ and $K_{MPPT} = 0$
2. The grid forming VSC and DC link dynamics model is already linear except the 8th-order model of the synchronous machine which is linearized according to small signal stability analysis (P.Kundur, 1994). The grid is modeled using Kirchoff's law in the d-q frame for line parameters R_g,L_g, and constant impedance load P_L

Hereafter for simplicity, the reference linear model is termed as linear model.

3.2 Simplified linear model

Using the same linearized model of the wind turbine, the simplified linearized model is developed based on following assumptions:

1. Considering that the energy stored in the capacitor is negligible compared with the energy stored in the inertia's, the dynamics of the DC voltage is neglected. Hence, the power P_G is considered as equal to P_{AC} using Eq.(15), it can be written as:

$$P_{AC} = P^*_G \tag{22}$$

2. All the AC system is considered in phasor with active power flow between voltage source P_{AC} and synchronous machine P_{SM} that depends on angle δ_m and δ_{SM} corresponding to voltage at grid forming converter v_m and synchronous machine v_{SM} respectively. The quasi-static representation of grid (Santos Pereira, 2020) with load P_L assuming voltage angles are small is :

$$\Delta P_{AC} = \frac{\Delta\delta_m - \Delta\delta_{SM}}{X_{AC} + X_{SM}} - \frac{X_{SM}\Delta P_L}{X_{AC} + X_{SM}} \tag{23}$$

$$\Delta P_{AC} = \frac{\Delta\delta_{SM} - \Delta\delta_m}{X_{AC} + X_{SM}} + \frac{X_{AC}\Delta P_L}{X_{AC} + X_{SM}} \tag{24}$$

https://doi.org/10.5194/wes-2025-10
Preprint. Discussion started: 31 January 2025

eawe european academy of wind energy
Open Access WIND ENERGY SCIENCE DISCUSSIONS

with $X_{AC} = L_c + L_g$ and $X_{SM} = L_c$, neglecting the resistance. These equations are used to obtain the network matrix $K_{network}$ as:

$$\begin{bmatrix} \Delta P_{AC} \\ \Delta P_{SM} \end{bmatrix} = \underbrace{\frac{1}{X_{AC} + X_{SM}} \begin{bmatrix} 1 & -1 & -X_{SM} \\ -1 & 1 & X_{AC} \end{bmatrix}}_{K_{network}} \begin{bmatrix} \Delta\delta_m \\ \Delta\delta_{SM} \\ \Delta P_L \end{bmatrix} \tag{25}$$

3. Simplified model of synchronous machine and governor: A second-order equivalent mechanical model is considered. All other internal dynamics are neglected. The damping coefficient $K_{d_{SM}}$ represents the combination of various damping effects of the system. Due to the non-linearity of the synchronous machine, its value is sensitive to the operating point.

The simplified linearized model of the system is illustrated in Fig.6. This model is only used to explain the different couplings in the system.

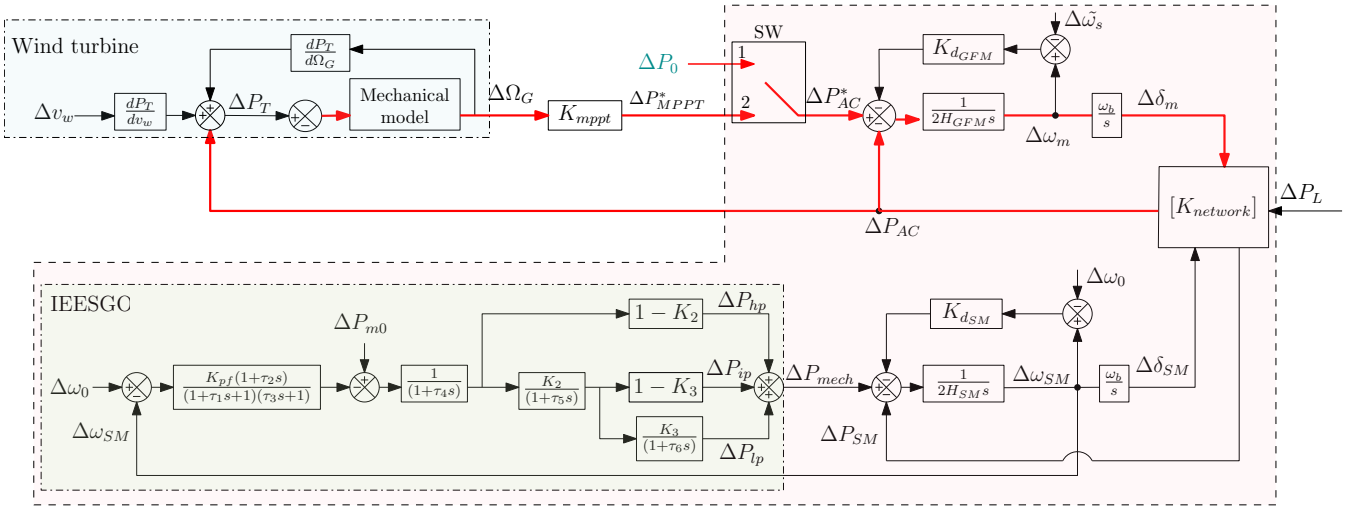

Figure 6. Simplified linearized model of the system

The dynamics of linear and simplified linear models are compared with the non-linear model for two operating points $P_1 = 0.67$ p.u. and $P_2 = 0.87$ p.u. corresponding to the MPPT zone1 and speed limitation zone2 showed in Fig.3b. Since the operating point of the synchronous machine is modified, the $K_{d_{SM}}$ value has to be adjusted: 30 p.u. for operating point P_1, 10 p.u. for operating point P_2. These values are obtained by the hit and trial method by comparing the dynamics with the non-linear model of the synchronous machine. The mechanical model of the wind turbine used is the one-mass model based on Eq.(10). The load step $\Delta P_L = 0.03$ p.u. is applied at 10 seconds, the variation in system dynamics is presented in Fig.7 and Fig.8 for operating point P_1 and P_2 respectively. Due to assumption Eq.(22) for the simplified linear model the variation in reference power Fig.7b and DC bus voltage Fig.7d contains results with linear model only.

Figure. 7b and 7e shows that after the load step, the unbalance between power delivered by GFM and generated by the wind

https://doi.org/10.5194/wes-2025-10
Preprint. Discussion started: 31 January 2025

eawe european academy of wind energy
Open Access WIND ENERGY SCIENCE DISCUSSIONS

turbine slows down the turbine. From Fig.7a and Fig.7b, it is observed that the dynamics of the active power aligns with its reference, thereby confirming the validity of Eq.(22). Whereas Fig.7d illustrates the small variation in DC bus voltage, also true for operating point P_2. Thus, only the variation in AC side power and wind turbine power is demonstrated in Fig.8 for P_2.Comparing wind turbine dynamics for two operating points Fig.7c and Fig.8b shows that due to the non-linearity in Eq.(11) and Eq.(12) there is a slight variation in ΔP_T in both linearized models. Further, comparing Fig.7a and Fig.8a it is observed that the inertial response provided by the GFM converter is more for operating point P_1.

The table 1 shows the dominant mode for different wind turbine models. It shows that the dominant frequency modes are reproduced by the simplified model even though $K_{d_{SM}}$ is different. Therefore, the linear models are validated and further sections provide more insight into the effect of variation in the operating region.

Model	Constant DC bus-grid forming	1-mass wind turbine-grid forming		2-mass wind turbine-grid forming	
		zone1	zone2	zone1	zone2
Linear	-0.22± 0.36j	-0.16±0.44j	-0.3±0.54j	-0.16±0.44j	-0.3±0.54j
Simplified linear	-0.23± 0.36j	-0.17±0.44j	-0.28±0.56j	-0.17±0.44j	-0.3±0.55j

Table 1. Comparative analysis of eigenvalues for different systems

4 Analysis of the influence of wind turbine on the system dynamics and improvements

4.1 Highlighting the main couplings in the system

The simplified linearized model shown in Fig.6 is considered to explain different couplings in the system. In case of a constant DC bus for the Grid Side VSC (Switch SW in position 1 with constant active power reference ΔP_0), this figure reveals a well-known interarea oscillations scheme similar to what can be found with 2 synchronous machines connected via a transmission grid (rose area in the Fig.6). The main difference is that the H_{GFM} and D_{GFM} are controlled variables which can be chosen by the control. Hence, the characteristics of the interarea oscillation modes in terms of frequency and damping can be strongly modified by the choice of these parameters [(Baruwa and Fazeli, 2021), (Xue et al., 2024)].

When SW is in position 2, the simplified linearized model shows that the wind turbine dynamics are modifying these oscillation modes. Indeed, an additional loop (in red in the system) is added in the system. This loop interacts with the previous modes and modifies the poles and damping as shown in Table 1. As can be shown in this table, the eigenvalue frequency increases and the damping is decreasing. With a physical insight, it can be understood that the wind turbine control tends to counteract the inertial effect brought to the grid by the GFM converter. Indeed, the signal P^*_{MPPT} is decreased by the control to recover the optimal rotational speed Ω_G. The effect of this additional loop is to decrease the energy that is exchanged with the grid and decrease the inertial effect. A possible solution to recover the expected inertial effect will be presented in the next

https://doi.org/10.5194/wes-2025-10
Preprint. Discussion started: 31 January 2025

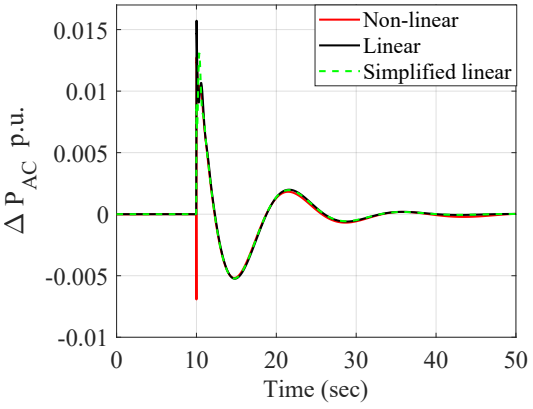

(a) Ac side power P_{AC}

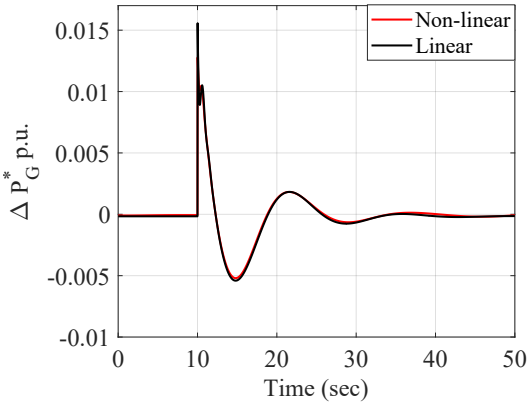

(b) Reference DC power P_G^*

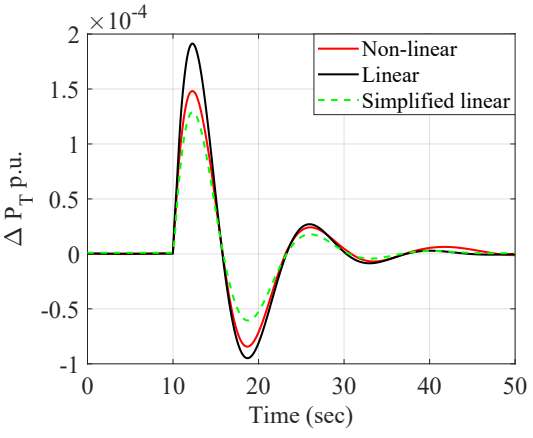

(c) Wind turbine power P_T

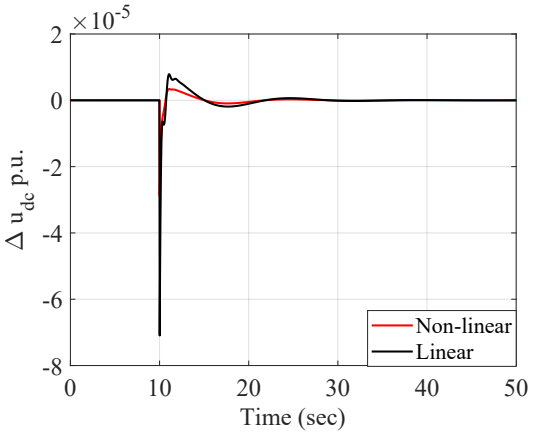

(d) DC voltage u_{dc}

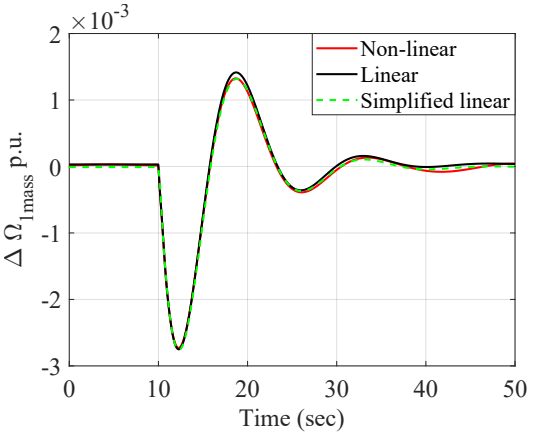

(e) Wind turbine speed Ω_{1mass}

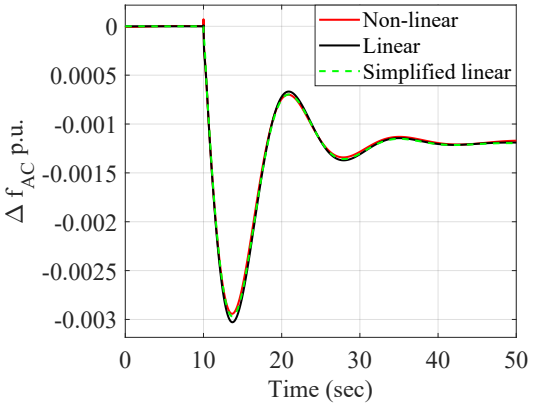

(f) Ac side frequency f_{AC}

Figure 7. Validation of linear models in zone1

https://doi.org/10.5194/wes-2025-10
Preprint. Discussion started: 31 January 2025

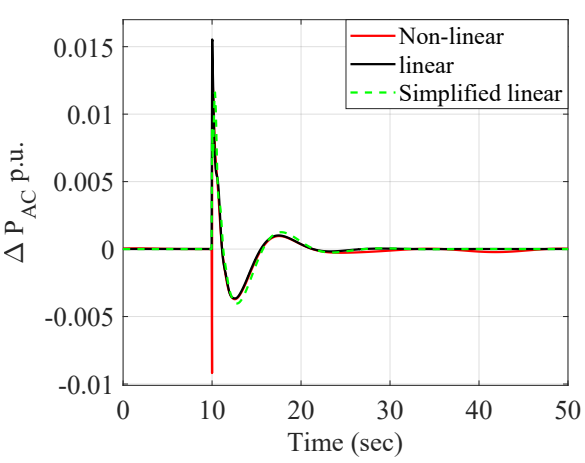

(a) Ac side power P_{AC}

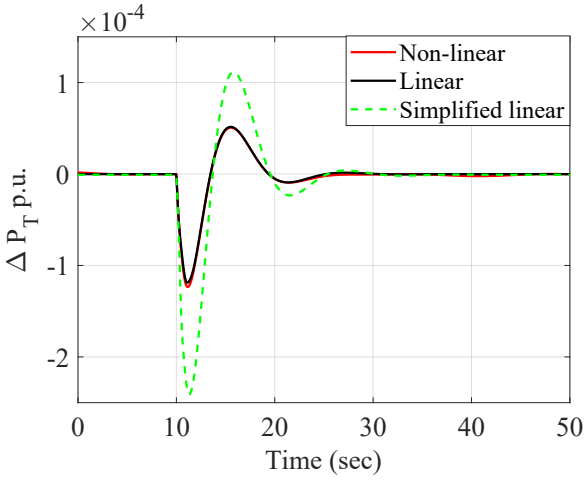

(b) Wind turbine power P_T

Figure 8. Validation of linear models in zone2

section. Due to the non-linearity of the loop, the dynamics is not the same depending on the operating point. The gain K_{MPPT} increased strongly between zone 1 and zone 2, consequently the dynamics increases also, see Table 1.

All these findings are confirmed by the simulation results shown in Fig.9 and obtained for a load step of 0.2 p.u.

It is also interesting to compare the dynamics of the system by using a one-mass or two-mass model for the drivetrain. The two-mass model offers a more comprehensive understanding of turbine dynamics, particularly in the low-frequency range. In Fig. 10a, a clear decoupling is observed between these eigenvalues and the oscillation modes of the wind turbine itself as the overall grid-side dynamics remain unaffected when employing either a one-mass model or a two-mass model in zone 1. However, in zone 2, where faster dynamics dominate as the equivalent gain K_{MPPT} is higher, the introduction of the two-mass model induces oscillatory behavior shown in Fig.10b.

This section highlights that connecting a wind turbine to a GFM converter introduces a new type of coupling. The undesirable phenomena identified can be mitigated by incorporating dedicated filters into the control loop. Two possible solutions are presented in the next sections.

4.2 Damping the mechanical oscillations using input shaping filter

In (Avazov, 2022), it was proposed to add an input shaping filter in the DC bus voltage control as shown in Fig.11. The principle of the input shaping is to modify a controlled reference signal by a convolution with a sequence of impulses to get a system response without oscillations as shown in Fig11. One type of these filters is known as a zero-vibration (ZV) filter allowing to achieve the zero level of residual vibrations (Huey et al., 2008). The design of the filter depends on the number of pulses, their amplitude (A_k), and the time of occurrence (t_k). A 2-pulse ZV filter can be expressed with amplitude A_1, A_2 and time t_1, t_2 in

https://doi.org/10.5194/wes-2025-10
Preprint. Discussion started: 31 January 2025

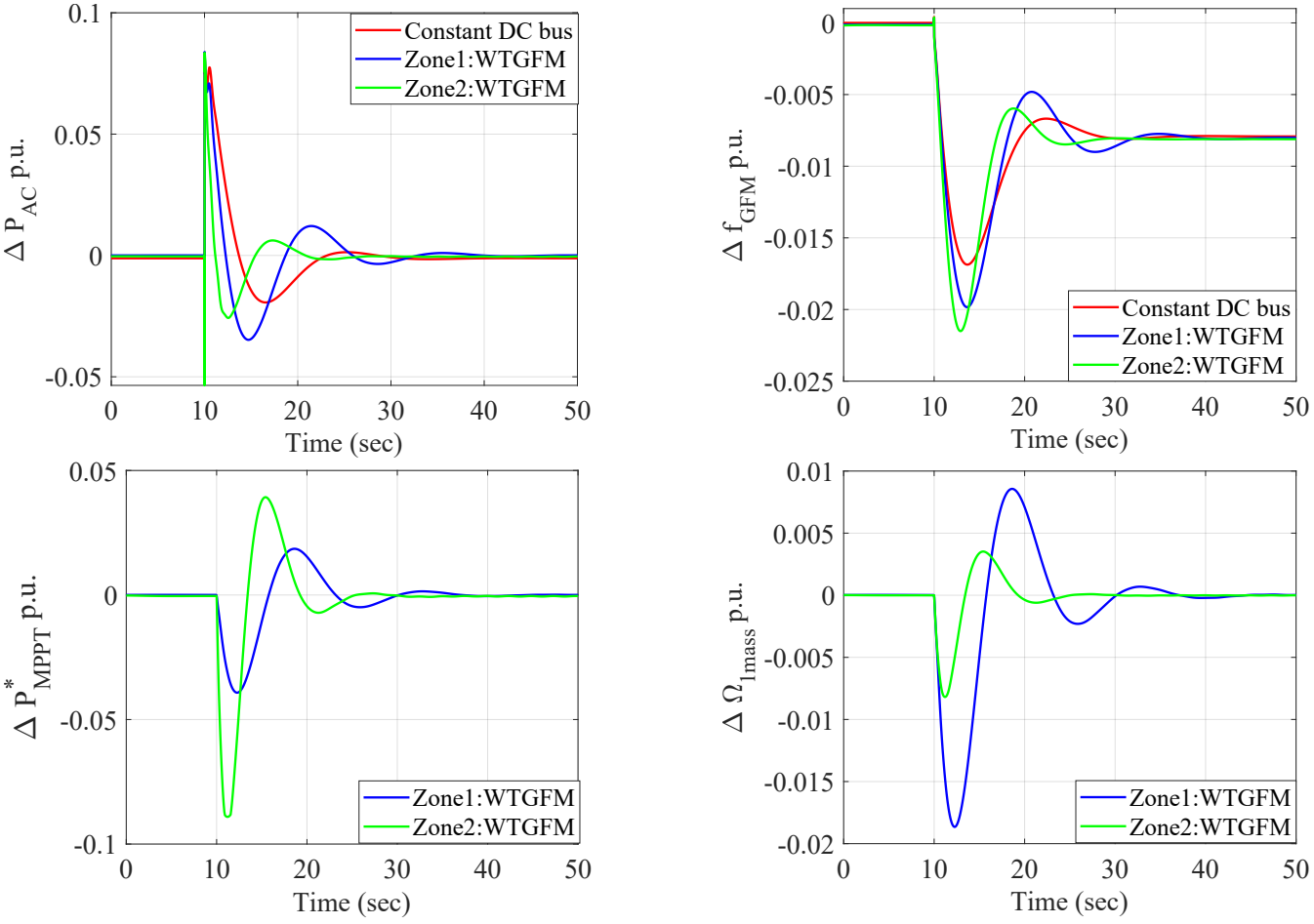

Figure 9. Inertial effect and frequency response of system with 1-mass wind turbine

Laplace domain:

$$IS(s) = A_{1f}e^{-t_1 s} + A_{2f}e^{-t_2 s} \tag{26}$$

with the necessary requirements as $0 \leqslant t_1 < t_2$ and $A_{1f} + A_{2f} = 1$.

The resulting finite impulse response filter formed can reduce vibrations in the mechanical system with the drivetrain oscillatory frequency ω_{damp} corresponding to drivetrain oscillatory mode $s = \sigma + j\omega_{damp}$ as follows:

$$t_1 = 0 \; ; \; t_2 = t_1 + \frac{\pi}{\omega_{damp}} \tag{27}$$

Thus, the pulse amplitudes are determined from drivetrain mode are:

$$A_1 = \frac{e^{\frac{\zeta\pi}{\sqrt{1-\zeta^2}}}}{1 + e^{\frac{\zeta\pi}{\sqrt{1-\zeta^2}}}} \; ; \; A_2 = 1 - A_1 \tag{28}$$

https://doi.org/10.5194/wes-2025-10
Preprint. Discussion started: 31 January 2025

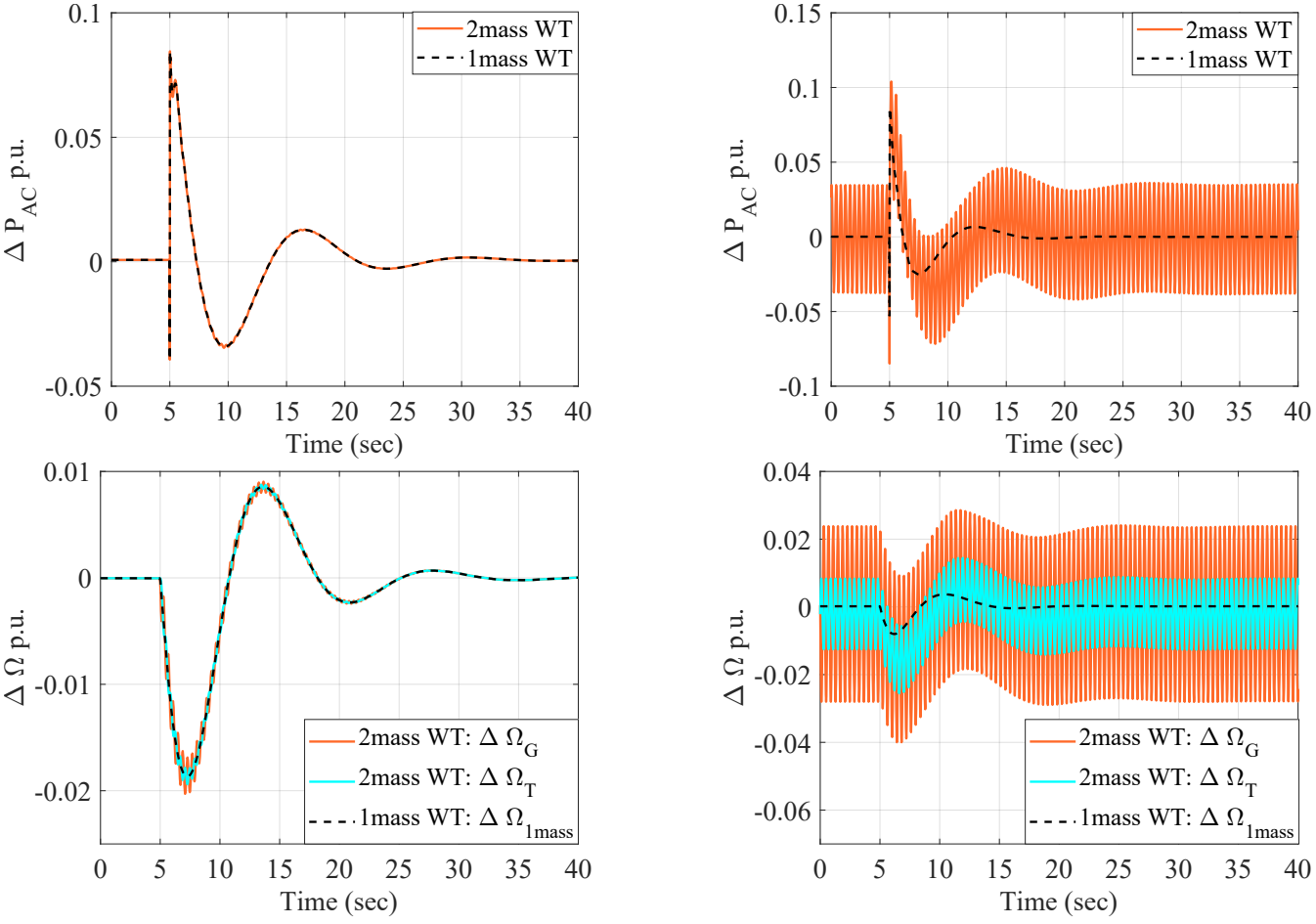

(a) Zone1

(b) Zone2

Figure 10. Analysis based on different mechanical system of wind turbine for load step of 0.2 p.u.

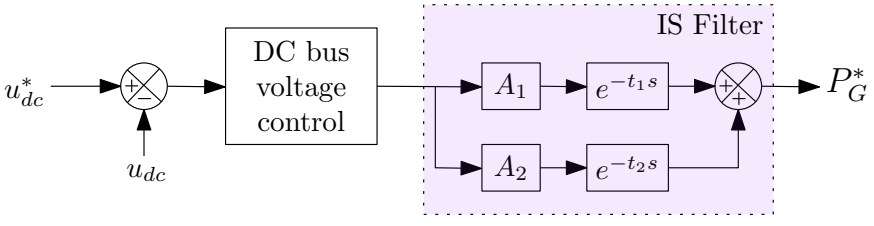

Figure 11. DC bus voltage control and input shaping filter

The limitation of this method is to introduce quite a large delay in the control since t_2 is quite large and depends on a low frequency mechanical mode. As it has been shown that the energy stored in the capacitor is negligible, the power P_G is nearly

https://doi.org/10.5194/wes-2025-10
Preprint. Discussion started: 31 January 2025

eawe european academy of wind energy
Open Access WIND ENERGY SCIENCE DISCUSSIONS

equal to P_{AC}, another solution is then to place this input shaping filter to generate the reference of the active power shown in Fig.12.

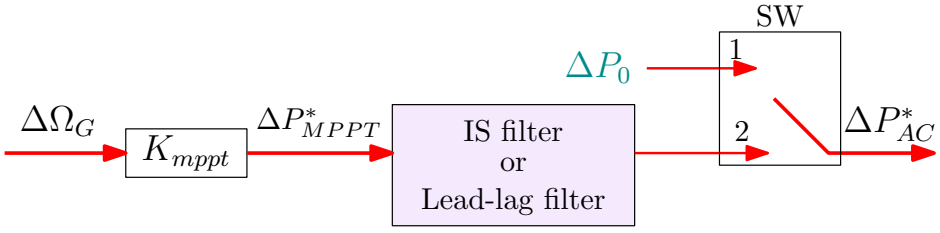

Figure 12. Proposed solution: Integration of filter in the system

Fig.13 shows the performance of this method since the mechanical oscillations are well damped by the input shaping filter and the system with the 2-mass model and the input shaping control behaves nearly as a 1-mass model.

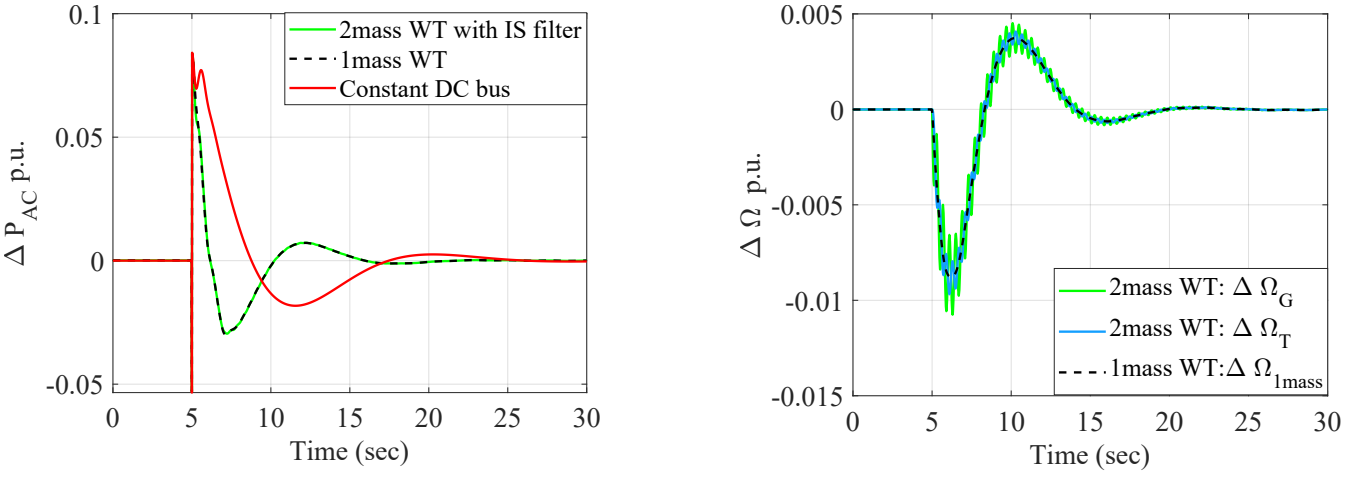

Figure 13. Effect of input shaping filter in zone2

4.3 Use of a lead lag filter to increase the inertial effect

As described before, the inertial response of a GFM controlled wind turbine is different from GFM controlled VSC with a constant DC bus. To enhance the inertial response of the GFM wind turbine, the MPPT control operation can be deliberately delayed through the implementation of a low-pass filter. This approach serves to smooth the power reference signal, effectively decoupling the GFM inertial effect from the mechanical dynamics of the wind turbine. By introducing this delay, the system mitigates rapid fluctuations in power demand that could otherwise interfere with the turbine's mechanical stability. Additionally, this strategy ensures a more predictable inertial contribution, thereby improving the overall behavior of the wind turbine in

https://doi.org/10.5194/wes-2025-10
Preprint. Discussion started: 31 January 2025

eawe european academy of wind energy
Open Access WIND ENERGY SCIENCE DISCUSSIONS

response to grid disturbances. This additional low-pass filter is expressed in Eq. (29).

$$\frac{P^*_{MPPT}}{P_{MPPT}} = \frac{1}{1+t_d s} \tag{29}$$

To tune correctly this filter, the system reponse has been tested for various lag coefficients (t_d) at P_1 for load step of 0.2 p.u. at 10 sec. The analysis in Fig.14a shows that using a t_d =20 sec low-pass first-order filter provides an improved inertial effect and the frequency response of the AC tends to be the same as with a constant DC bus voltage. It may be possible to increase the filter time constant to 30 seconds, but this would result in slower mechanical modes. In any case, the mechanical counterpart is a larger speed variation of the wind turbine which can be explained since the wind turbine provide more inertial effect to the grid.

As it can be shown on Fig.14a, adding a filter tends to decrease the damping of the dominant mode. A possible solution is to add a lead effect Eq.(30) to improve the transient response.

$$\frac{P^*_{MPPT}}{P_{MPPT}} = \frac{1+t_n s}{1+t_d s} \tag{30}$$

The system is tested for various lead coefficients (t_n) in zone 1 while keeping the delay $t_d = 20$ sec. The choice is a trade off between the improvement of the damping of the mode and the decrease of the inertial effect. The resulting Fig.14b shows that $t_n = 4.5$ sec is an optimal choice.

When the tuning is achieved in zone 1, the effectiveness of the lead-lag filter in zone 2 has to be checked. As previously the large increase of the gain K_{MPPT} leads to a more oscillating behaviour, as seen on Fig.15, with no possibility to improve this damping. On this figure, it can be noticed that the drive train oscillations are well damped by the filter so there is no need to add the input shaping filter in series with the lead-lag filter.

5 Conclusions

The requirement for grid-forming behavior in wind turbines introduces a new type of coupling, as highlighted by the linearized system proposed in this paper. This model provides a clear understanding of how the dominant frequency mode is influenced by wind turbine dynamics and identifies the key parameters that affect this mode. Among these, the gain of the MPPT (Maximum Power Point Tracking) strategy emerges as a critical factor, as its value varies significantly depending on the operational zone.

Additionally, The analysis also underscores the importance of accounting for the internal mechanical dynamics of the wind turbine. Depending on the operating point, unwanted oscillations can appear in the rotational speed of the turbine. To address this, an active damping effect can be introduced to suppress oscillatory mechanical modes by incorporating an input-shaping filter to generate the active power reference. This approach is advantageous compared to previously proposed methods, as it avoids interference with the DC bus control dynamics and has a negligible impact on the active power dynamics of the wind turbine.

It has also been further revealed that the internal dynamics of the wind turbine influence the dominant frequency mode. This is due to the interaction between the MPPT control and active power management, as rapid modifications of the power

https://doi.org/10.5194/wes-2025-10
Preprint. Discussion started: 31 January 2025

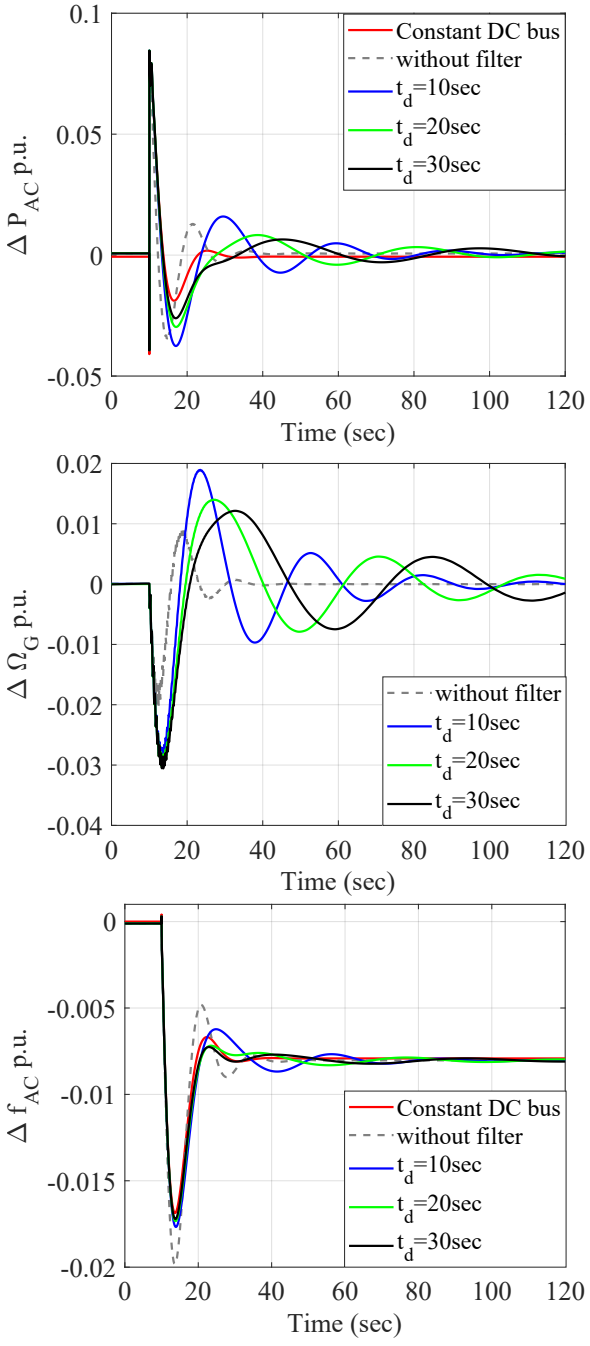

(a) Inertial response with lowpass filter in zone1

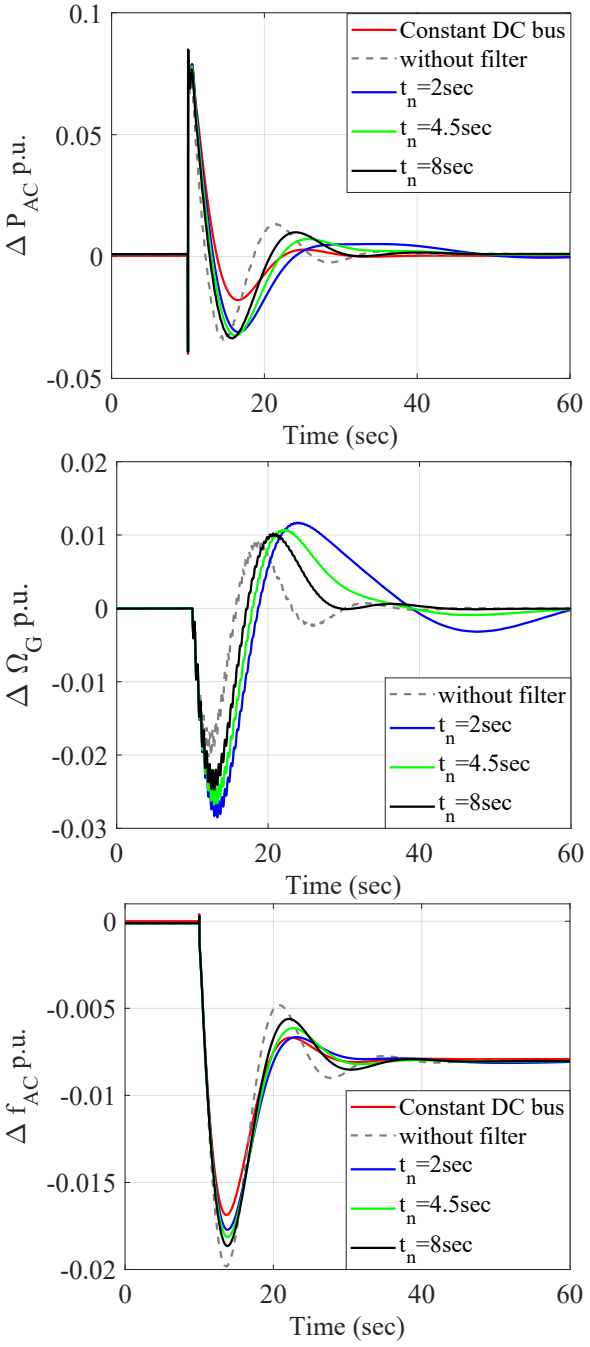

(b) Inertial response with lead-lag filter in zone1

Figure 14. Inertia enhancement with lowpass and leadlag filter for P_1

https://doi.org/10.5194/wes-2025-10
Preprint. Discussion started: 31 January 2025

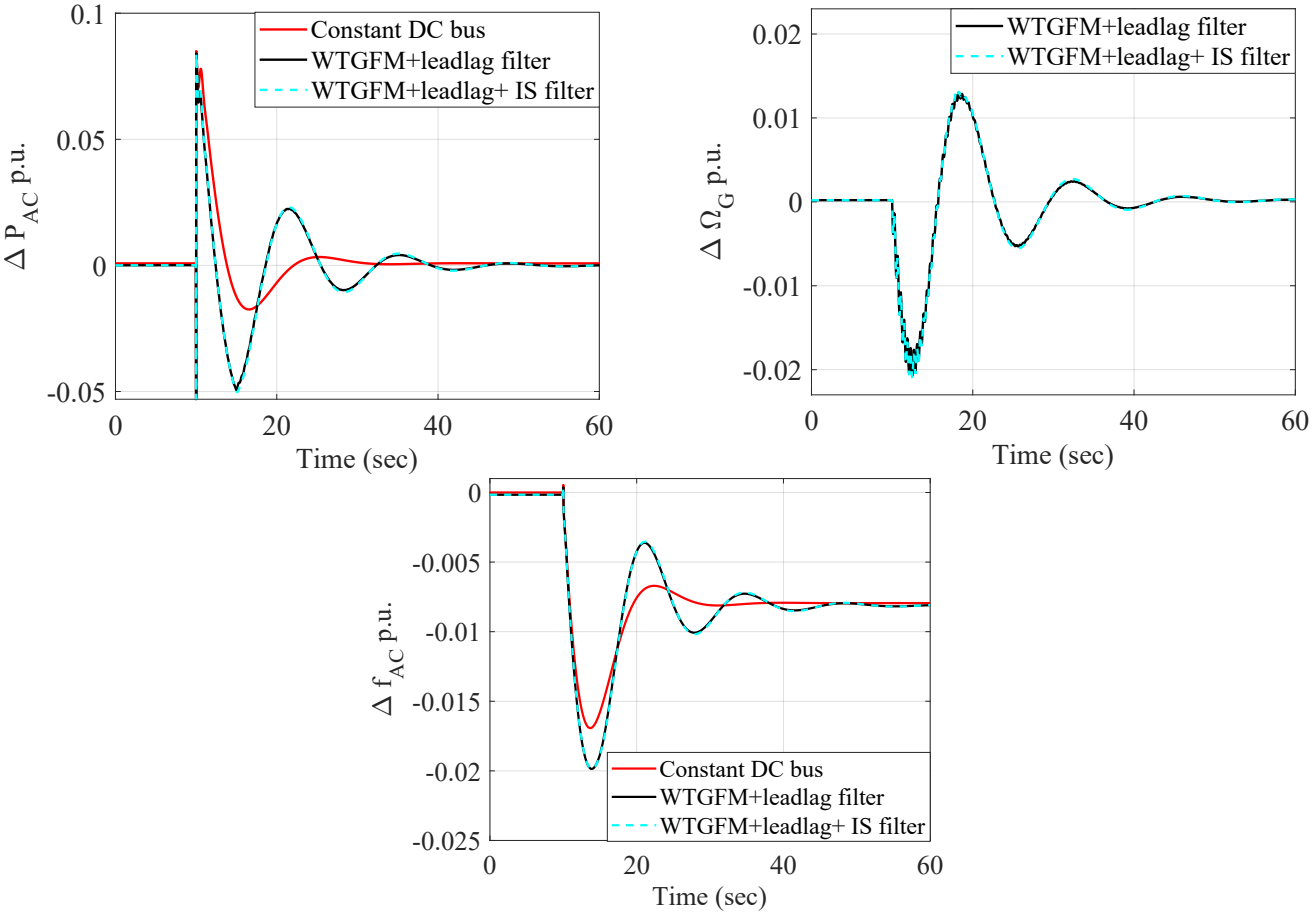

Figure 15. Inertial response in zone2 with leadlag filter

reference reduce the expected inertial effect of the grid-forming converter. A practical solution to mitigate this issue is also the addition of a filter in the control loop. This filter is a lead-lag one which, this time, decouples the system's dominant mode from the mechanical modes of the wind turbine. As expected, mechanical variations are more pronounced on the wind turbine side, where energy exchange with the grid is higher. In addition, the inclusion of this lead-lag action slightly dampens the observed
305 oscillatory behavior following a grid frequency variation.

This paper has given some general trends of the dynamics of Grid forming wind turbine connected to an AC grid but many work is still to be done to deepen this analysis. The mechanical model should be improved to ensure that the unmodeled modes do not induce additional interaction with the grid modes. Moreover, it is possible to implement other types of MPPT control and analyse if the same conclusion can be drawn.

https://doi.org/10.5194/wes-2025-10
Preprint. Discussion started: 31 January 2025

eawe european academy of wind energy
Open Access WIND ENERGY SCIENCE DISCUSSIONS

Appendix A: Parameters of the system

Parameter	Value
S_{nom}	900MVA
f_{nom}	50 Hz
U_{nom}	400kV
R_g	0.02 p.u.
L_g	0.2 p.u.

(a) System parameters

Parameter	Value
$V_{dc_{nom}}$	640kV
H_{dc}	40msec
ζ_{dc}	0.7
$T_{r_{dc}}$	0.5 sec

(b) Dc voltage control parameters

Table A1. System parameters

Parameter	Value
H_{GFM}	4.5 sec
ζ_{GFM}	0.7
$K_{d_{GFM}}$	192 p.u.
R_c	0.005 p.u.
L_c	0.15 p.u.
R_v	0.09
ω_f	60 Hz

(a) Grid forming converter

Parameter	Value
P_{nom}	5MW
N_{wt}	180
ω_{nom}	1.1905 rad/sec
H_T	1.93 sec
H_G	0.8 sec
K_s^{pu}	280 p.u.
D_s^{pu}	1
λ_{opt}	7
$c_{p_{opt}}$	0.44
R	63 m
ρ	1.22

(b) Wind turbine parameters

Table A2. Wind turbine-grid forming parameters

https://doi.org/10.5194/wes-2025-10
Preprint. Discussion started: 31 January 2025

eawe european academy of wind energy
Open Access WIND ENERGY SCIENCE DISCUSSIONS

Parameter	Value
H_{SM}	6.5 sec
X_d	1.8
X_q	1.7
X_l	0.2
$X_d^{'}$	0.3
$X_d^{''}$	0.25
$X_q^{'}$	0.55
$X_q^{''}$	0.25
$T_d^{'}$	8
$T_d^{''}$	0.03
$T_q^{'}$	0.4
$T_q^{''}$	0.05

(a) Electrical parameters

Parameter	Value
K_{pf}	-25
K_2	0.7
K_3	0.4
τ_1	0.1 sec
τ_2	0 sec
τ_3	0.2 sec
τ_4	0.05 sec
τ_5	7.0 sec
τ_6	0.4 sec
K_a	200
τ_r	0.01

(b) IEESGO and excitation system parameters

Table A3. Synchronous machine parameters

Parameter	Value
A_1	0.54
A_2	0.46
t_1	0
t_2	0.2 sec

Parameter	Value
t_n	4.5 sec
t_d	20 sec

Table A4. Filter parameters

Author contributions. CW implemented the test case in MATLAB, with JB contributing to the wind turbine-grid forming modeling, LR to the modeling of the synchronous machine, and FC to the implementation of the input-shaping filter. The study was conceptualized by XG and FC. CW and XG prepared the manuscript, with contributions from all co-authors.

Competing interests. The authors declare that they have no conflict of interest.

Acknowledgements. The authors gratefully acknowledge the Région Hauts-de-France for funding this project.

https://doi.org/10.5194/wes-2025-10
Preprint. Discussion started: 31 January 2025

eawe european academy of wind energy
Open Access WIND ENERGY SCIENCE DISCUSSIONS

References

IEEE Recommended Practice for Excitation System Models for Power System Stability Studies, IEEE Std 421.5-2016 (Revision of IEEE Std 421.5-2005), pp. 1–207, https://doi.org/10.1109/IEEESTD.2016.7553421, 2016.

Avazov, A.: AC Connection of Wind Farms to Transmission System : from Grid-Following to Grid-Forming, Theses, Centrale Lille Institut ; Katholieke universiteit te Leuven (1970-....). Faculteit Geneeskunde, https://theses.hal.science/tel-04074095, 2022.

Baruwa, M. and Fazeli, M.: Impact of Virtual Synchronous Machines on Low-Frequency Oscillations in Power Systems, IEEE Transactions on Power Systems, 36, 1934–1946, https://doi.org/10.1109/TPWRS.2020.3029111, 2021.

Cardozo, C., Prevost, T., Huang, S.-H., Lu, J., Modi, N., Hishida, M., Li, X., Abdalrahman, A., Samuelsson, P., Cutsem, T. V., Laba, Y., Lamrani, Y., Colas, F., and Guillaud, X.: Promises and challenges of grid forming: Transmission system operator, manufacturer and academic view points, Electric Power Systems Research, 235, 110 855, https://doi.org/https://doi.org/10.1016/j.epsr.2024.110855, 2024.

Chen, L., Du, X., Hu, B., and Blaabjerg, F.: Drivetrain Oscillation Analysis of Grid Forming Type-IV Wind Turbine, IEEE Transactions on Energy Conversion, 37, 2321–2337, https://doi.org/10.1109/TEC.2022.3179609, 2022.

ENTSOE: High Penetration of Power Electronic Interfaced Power Sources (HPoPEIPS), Tech. rep., https://consultations.entsoe.eu/system-development/entso-e-connection-codes-implementation-guidance-d-3/user_uploads/igd-high-penetration-of-power-electronic-interfaced-power-sources.pdf, 2017.

ESO: Great Britain Grid Forming Best Practice Guide, https://www.studocu.com/pt-br/document/escola-universitaria-universidade-federal-do-rio-de-janeiro/ciencias/great-britain-grid-forming-best-practices-guide-april-2023/92650440, 2023.

Heidary Yazdi, S. S., Milimonfared, J., Fathi, S. H., Rouzbehi, K., and Rakhshani, E.: Analytical modeling and inertia estimation of VSG-controlled Type 4 WTGs: Power system frequency response investigation, International Journal of Electrical Power & Energy Systems, 107, 446–461, https://doi.org/https://doi.org/10.1016/j.ijepes.2018.11.025, 2019.

Hu, J., Wang, S., Tang, W., and Xiong, X.: Full-Capacity Wind Turbine with Inertial Support by Adjusting Phase-Locked Loop Response, IET Renewable Power Generation, 11, 44–53, https://doi.org/https://doi.org/10.1049/iet-rpg.2016.0155, 2016.

Huang, L., Wu, C., Zhou, D., Chen, L., Pagnani, D., and Blaabjerg, F.: Challenges and potential solutions of grid-forming converters applied to wind power generation system—An overview, Frontiers in Energy Research, 11, https://doi.org/10.3389/fenrg.2023.1040781, 2023.

Huey, J. R., Sorensen, K. L., and Singhose, W. E.: Useful applications of closed-loop signal shaping controllers, Control Engineering Practice, 16, 836–846, https://doi.org/https://doi.org/10.1016/j.conengprac.2007.09.004, 2008.

Krpan, M. and Kuzle, I.: Introducing low-order system frequency response modelling of a future power system with high penetration of wind power plants with frequency support capabilities, IET Renewable Power Generation, 12, 1453–1461, https://doi.org/https://doi.org/10.1049/iet-rpg.2017.0811, 2018.

Lamrani, Y., Colas, F., Van Cutsem, T., Cardozo, C., Prevost, T., and Guillaud, X.: Investigation of the Stabilizing Impact of Grid-Forming Controls for LCL-connected Converters, in: 2023 25th European Conference on Power Electronics and Applications (EPE'23 ECCE Europe), pp. 1–8, https://doi.org/10.23919/EPE23ECCEEurope58414.2023.10264339, 2023.

Morren, J., Pierik, J., and de Haan, S. W.: Inertial response of variable speed wind turbines, Electric Power Systems Research, 76, 980–987, https://doi.org/https://doi.org/10.1016/j.epsr.2005.12.002, 2006.

P.Kundur: Power System Stability and Control, McGraw- Hill, New York, 1994.

https://doi.org/10.5194/wes-2025-10
Preprint. Discussion started: 31 January 2025

Pourbeik, P., Chown, G., Feltes, J., Modau, F., Sterpu, S., Boyer, R., Chan, K., Hannett, L., Leonard, D., Lima, L., Hofbauer, W., Gerin-Lajoie, L., Patterson, S., Undrill, J., and Langenbacher, F.: Dynamic Models for Turbine-Governors in Power System Studies, 2013.

Ramasubramanian, D., Kroposki, B., Dhople, S., Groß, D., Hoke, A., Wang, W., Shah, S., Hart, P., Seo, G.-S., Ropp, M., Du, W., Vittal, V., Ayyanar, R., Flicker, J., Benzaquen, J., Johnson, B., Arsuaga, P., Achilles, S., Pant, S., Bhattarai, R., Howard, D., Gong, M., Divan, D., and Tuohy, A.: Performance Specifications for Grid-forming Technologies, in: 2023 IEEE Power & Energy Society General Meeting (PESGM), pp. 1–5, https://doi.org/10.1109/PESGM52003.2023.10253440, 2023.

Rathnayake, D. B., Akrami, M., Phurailatpam, C., Me, S. P., Hadavi, S., Jayasinghe, G., Zabihi, S., and Bahrani, B.: Grid Forming Inverter Modeling, Control, and Applications, IEEE Access, 9, 114 781–114 807, https://doi.org/10.1109/ACCESS.2021.3104617, 2021.

Rosso, R., Wang, X., Liserre, M., Lu, X., and Engelken, S.: Grid-Forming Converters: Control Approaches, Grid-Synchronization, and Future Trends—A Review, IEEE Open Journal of Industry Applications, 2, 93–109, https://doi.org/10.1109/OJIA.2021.3074028, 2021.

Santos Pereira, G.: Stability of power systems with high penetration of sources interfaced by power electronics, Theses, Centrale Lille Institut, https://theses.hal.science/tel-03267852, 2020.

Shafiu, A., Anaya-Lara, O., Bathurst, G., and Jenkins, N.: Aggregated Wind Turbine Models for Power System Dynamic Studies, Wind Engineering, 30, 171–185, https://doi.org/10.1260/030952406778606205, 2006.

Tessaro, H. J. and de Oliveira, R. V.: Impact assessment of virtual synchronous generator on the electromechanical dynamics of type 4 wind turbine generators, IET Generation, Transmission & Distribution, 13, 5294–5304, https://doi.org/https://doi.org/10.1049/iet-gtd.2019.0818, 2019.

Wu, Z., Gao, W., Wang, X., Kang, M., Hwang, M., Kang, Y. C., Gevogian, V., and Muljadi, E.: Improved inertial control for permanent magnet synchronous generator wind turbine generators, IET Renewable Power Generation, 10, 1366–1373, https://doi.org/https://doi.org/10.1049/iet-rpg.2016.0125, 2016.

Wu, Z., Gao, W., Gao, T., Yan, W., Zhang, H., Yan, S., and Wang, X.: State-of-the-art review on frequency response of wind power plants in power systems, Journal of Modern Power Systems and Clean Energy, 6, 1–16, https://doi.org/10.1007/s40565-017-0315-y, 2018.

Xi, J., Geng, H., Ma, S., Chi, Y., and Yang, G.: Inertial response characteristics analysis and optimisation of PMSG-based VSG-controlled WECS, IET Renewable Power Generation, 12, 1741–1747, https://doi.org/https://doi.org/10.1049/iet-rpg.2018.5250, 2018.

Xue, T., Zhang, J., and Bu, S.: Inter-Area Oscillation Analysis of Power System Integrated With Virtual Synchronous Generators, IEEE Transactions on Power Delivery, 39, 1761–1773, https://doi.org/10.1109/TPWRD.2024.3376523, 2024.